[CANCER RESEARCH 63, 7232–7240, November 1, 2003]

An Integrated Approach to Measuring Tumor Oxygen Status Using Human Melanoma Xenografts as a Model[1]

Chandrakala Menon,[2] Glenn M. Polin,[2] Indira Prabakaran, Alex Hsi, Cecil Cheung, Joseph P. Culver, James F. Pingpank, Chandra S. Sehgal, Arjun G. Yodh, Donald G. Buerk, and Douglas L. Fraker[3]

Departments of Surgery [C. M., G. M. P., I. P., J. F. P., D. L. F.], Radiation Oncology [A. H.], Physics and Astronomy [C. C., J. P. C., A. G. Y.], Radiology [C. S. S.], and Physiology [D. G. B.], University of Pennsylvania, Philadelphia, Pennsylvania 19104

ABSTRACT

Tumor oxygen status is a reliable prognostic marker that impacts malignant progression and outcome of tumor therapy. However, tumor oxygenation is heterogeneous and cannot be sufficiently described by a single parameter. It is influenced by several factors including microvessel density (MVD), blood flow (BF), blood volume (BV), blood oxygen saturation, tissue pO_2, oxygen consumption rate, and hypoxic fraction. The goal of this investigation was to integrate these measurements to obtain a comprehensive profile of tumor oxygenation. Platelet/endothelial cell adhesion molecule immunohistochemistry, the recessed oxygen microelectrode, color and power Doppler ultrasound (DUS), and diffuse light spectroscopy (DLS) were used to measure tumor oxygen status using vascular endothelial growth factor (VEGF)-transfected hypervascular human melanoma xenografts and their nontransfected counterparts as a model. NIH1286 human melanoma cells were transfected with a retroviral vector ± a 720-bp fragment of human $VEGF_{121}$. High VEGF-producing clones were selected by ELISA. Oxygen consumption rate was measured in NIH1286/VEGF+ [VEGF-transfected cells (VEGF+ cells)] and NIH1286/Vec cells [cells transfected with vector alone (Vec cells)] using a standard Clark oxygen electrode. Athymic nude 6–8-week-old mice received s.c. injection in the right flank with 5×10^6 VEGF+ or Vec cells. When tumors were 10–14 mm in maximum dimension, serum was analyzed for VEGF by ELISA. Cryopreserved tumor tissue sections were immunostained for platelet/endothelial cell adhesion molecule, and MVD measurements were made. Tumor-bearing mice were anesthetized, and pO_2 measurements were made using Eppendorf pO_2 histograph or the recessed oxygen microelectrode. Tumor BF and BV were measured by quantitative analysis of DUS images. DLS was used to measure tumor BF and blood oxygen saturation variation. VEGF+ cell supernatants had 15,500 pg/ml VEGF, and Vec cells had 10 pg/ml. VEGF+ and Vec cells had equivalent oxygen consumption rates. VEGF+ tumors had a faster growth rate than Vec tumors. Serum from VEGF+ tumor-bearing mice showed 4,211 pg/ml VEGF, whereas VEGF was undetectable in the serum of control mice. MVD values were 74 ± 11 in VEGF+ tumors and 39 ± 4 in control tumors at ×200 magnification/0.95-mm^2 area. The median pO_2 values were 3.5-fold higher in VEGF+ tumors than in Vec tumors by the recessed oxygen microelectrode and 18-fold higher by Eppendorf pO_2 histograph. DUS showed a 3.3-fold higher mean BF and a 5.5-fold higher BV in VEGF+ tumors than in Vec tumors. DLS showed a 3.2-fold higher mean BF and 1.7-fold higher oxygen saturation in the hypervascular tumors as compared with the control tumor type, consistent with increased BF and BV data by DUS. An integrated approach that yields a comprehensive and consistent profile of oxygen status in tumors could potentially provide critical information for prognosis and treatment.

INTRODUCTION

The physiology of solid tumors differs from that of normal tissues primarily because of consistent differences between tumor and normal microvasculature. Compared with the regular, ordered vasculature of normal tissues, blood vessels in tumors are often highly abnormal, with distended capillaries, leaky walls, and sluggish flow (1). Hypoxic regions are thus typical of virtually all solid tumors. There is significant intertumoral and intratumoral variability in the extent of hypoxia. In addition, local recurrences have been known to have a higher hypoxic fraction than primary tumors (2). Tumor oxygen status appears to be strongly associated with tumor growth, malignant progression, and resistance to various therapies including radiotherapy, photodynamic therapy, and chemotherapy (3). It can also influence angiogenesis, cytokine production, cell cycle position of tumor cells, and the development of apoptosis/necrosis (3).

Tumor oxygen status plays a central role in tumor physiology and cancer treatment and is therefore a powerful independent prognostic factor of overall and disease-free survival. The routine evaluation of the pretherapeutic tumor oxygenation status may, in fact, facilitate the establishment of individual therapeutic strategies, independent of other oncologic parameters (4). Another area of importance in which measurement of tumor oxygen status can serve as an important end point is in the assessment of the efficacy of agents classified as antiangiogenic compounds, agents that target the tumor vasculature rather than cause direct cytotoxicity to malignant cells (5). Investigators have argued that the standard measure of response in terms of tumor size is not suitable when evaluating these agents and that studies should use parameters associated with the tumor vasculature, especially those related to tumor oxygenation status, as the end point.

Many independent studies involving different techniques have measured one or more parameters to define tumor oxygen status. These techniques include phosphorescence lifetime (quench) imaging (6) to measure oxygen diffusion distances between tumor microvessels (7) and evaluate longitudinal tissue gradients of oxygen (8), magnetic resonance imaging to monitor vascular oxygenation and BF[4] (9), cryospectrophotometry to measure hemoglobin saturation (10), single-photon emission computed tomography and positron-emission tomography assays to measure perfusion and mark hypoxic areas (11–13), injection of Hoechst 33342, a DNA-binding dye that marks the presence of functional vessels (14), and the use of hypoxia markers to identify hypoxic tumor regions (15). Whereas these studies have provided important information, they have also shown that tumor oxygenation is quite heterogeneous, so that an assessment combining several different methods is desirable to define the oxygen profile of a tumor for diagnostic and prognostic purposes. Also, such a combination of techniques will provide validation of the measurements while giving a more accurate overall tumor oxygenation profile. The clinically relevant oxygen status of a tumor is defined by a number of related parameters such as MVD, BF, total BV, blood OS, tumor tissue pO_2, hypoxic fraction, oxygen consumption rate, and oxygen diffusion distance. This work has adopted an integrated approach to

Received 2/11/03; revised 8/7/03; accepted 8/18/03.

The costs of publication of this article were defrayed in part by the payment of page charges. This article must therefore be hereby marked *advertisement* in accordance with 18 U.S.C. Section 1734 solely to indicate this fact.

[1] Supported in part by the Georgene S. Harmelin Endowment Fund.

[2] Both authors contributed equally to this work.

[3] To whom requests for reprints should be addressed, at Hospital of the University of Pennsylvania, 4 Silverstein Building, 3400 Spruce Street, Philadelphia, PA 19104. Phone: (215) 662-7866; Fax: (215) 614-0765; E-mail: Frakerd@uphs.upenn.edu.

[4] The abbreviations used are: BF, blood flow; MVD, microvessel density; BV, blood volume; OS, oxygen saturation; PECAM, platelet/endothelial cell adhesion molecule; DUS, Doppler ultrasound; DLS, diffuse light spectroscopy; VEGF, vascular endothelial growth factor; hVEGF, human VEGF; VD, vascular density; MCL, mean color level; CWFA, color-weighted fractional area; NIR, near-infrared.

define tumor oxygen status using a VEGF-transfected human melanoma xenograft and its vector-only transfected control tumor as a model. Specifically, the work reports MVD measurements, recessed microelectrode measurements (pO_2), color (BF), and power (BV) Doppler measurements and DLS measurements (BF and OS). An integrated approach, using a limited number of complementary techniques that yield overlapping data that validate each other, can potentially be used to generate clinically relevant information on tumor oxygen status in a variety of tumors types. Such information can then be used not only as a prognostic tool but also as the basis for developing and evaluating patient-specific treatment modalities for many types of cancers.

MATERIALS AND METHODS

Cell Lines and Culture Conditions. The NIH1286 human melanoma cell line, a generous gift from Dr. Steven Rosenberg (NIH, Bethesda, MD), was grown in RPMI 1640 supplemented with 10% FCS, 2 mM L-glutamine, 100 units/ml penicillin, and 100 μg/ml streptomycin (all obtained from Life Technologies, Inc., Gaithersburg, MD). PA317 retroviral packaging cell line (American Type Culture Collection, Manassas, VA) was cultured in DMEM (Life Technologies, Inc.) supplemented with the above-mentioned additives.

Cloning of the VEGF Gene. PSL301 vector containing a 720-bp fragment of $hVEGF_{121}$ (a generous gift from Dr. Meenhard Herlyn; Wistar Institute, Philadelphia, PA) was digested with *Not*I and cloned into the *Not*I site of retroviral vector PG1EN, which was obtained from Dr. Patrick Hwu (National Cancer Institute, Bethesda, MD). PG1EN VEGF or PG1EN DNA was transfected using LipofectAMINE (Life Technologies, Inc.) into the packaging cell line, PA317. A heterogeneous population of PA317 containing PG1EN-VEGF (PLVh121EN) or PG1EN vector alone was selected with G418 (200 μg/ml; Life Technologies, Inc.). Virus was harvested from these stable packaging cell lines and used to transduce the melanoma cell line NIH1286. Single cell clones were selected using 400 μg/ml G418.

Screening of VEGF and Vector-Only Clones by PCR. DNA was extracted from the selected single cell clones and screened for VEGF insert by PCR.

DNA Extraction. Cells (500,000) were washed in PBS, pelleted, and resuspended in 200 μl of proteinase K buffer containing 1 ml of 10× PCR buffer (Boehringer Mannheim), 9 ml of deionized water, 50 μl of Tween 20 (Sigma), and 20 μg of proteinase K (Sigma). The solution was incubated at 55°C for 2 h, boiled for 5 min, placed on ice for 2 min, and centrifuged at 300 × *g*. Two μl of supernatant were used for the PCR reaction.

PCR for VEGF Plus Vector or Vector Alone. PCR was carried out in a 100-μl volume containing 200 μM deoxynucleotide triphosphates, 1 unit of Taq polymerase, and PCR buffer (all purchased from Roche Molecular Biochemicals), and 0.25 μM each of the upstream and downstream primers was used. The reaction was allowed to run for 35 cycles. Each cycle had the following settings: 94°C for 1 min; 53°C for 1 min; and 72°C for 1 min. The upstream primer sequence for VEGF plus vector was 5′-AGG-AGG-AGG-GCA-GAA-TCA-TCA-C-3′, and the downstream primer sequence was 5′-TTT-GGC-GAG-AGG-GGA-AAG-AC-3′. The downstream primer chosen was in the vector region to avoid expression of endogenous VEGF. The primer sequences for the vector alone were 5′-ATG-ATT-GAA-CAA-GAT-GGA-TTG-GAC-G-3′ (Neofor) and 5′-TCA-GAA-GAA-CTC-GTC-AAG-AAG-GCG-A-3′ (Neoback). The annealing temperature for the vector alone PCR reaction was 56°C. PCR products were electrophoresed on a 1.2% agarose gel in 1× tris acetate EDTA buffer and stained with ethidium bromide.

Selection of High VEGF Protein-Producing Clones by ELISA. Clones positive by PCR for VEGF transgene were assayed for protein production using a Quantikine hVEGF ELISA kit (R&D Systems Inc., Minneapolis, MN). Briefly, 100,000 cells of each selected clone were plated on 24-well plates and incubated for 24 h in RPMI 1640. Supernatants were harvested and assayed for hVEGF.

Determination of Oxygen Consumption Rate in VEGF+/Vec Cells. Oxygen consumption in the two cell types was measured using a standard Clark oxygen electrode. Briefly, the electrodes were allowed to incubate in the air-tight incubation chamber with 2.8 ml of 50 mM HEPES buffer (pH 7.4) at 37°C for a period of 10 min, until a steady baseline was obtained on the chart. VEGF+ or Vec cells were suspended in 50 mM HEPES buffer (pH 7.4) at 37°C, and 200 μl of a 1×10^6 cells/ml sample were introduced into the incubation chamber using a syringe through the side arm of the chamber. Oxygen consumption was calculated and expressed as nmol oxygen consumed/min/10^5 cells in the air-tight chamber under continuous stirring.

Tumor Production in Nude Mice. Athymic nude mice (Harlan Sprague Dawley, Indianapolis, IN) were housed in the Animal Care Facility at the University of Pennsylvania according to NIH and institutional guidelines. At 6–8 weeks of age, the mice received s.c. injection with 5×10^6 NIH1286/Vec (vector alone; Vec cells) or NIH1286/VEGF+ cells (VEGF+ cells) in 0.1 ml of RPMI 1640. The latter clone was derived from the high VEGF-expressing cell lines that were selected based on *in vitro* cell supernatant ELISA assays for VEGF. Tumors were allowed to grow over the next 3–6 weeks until they reached 10 mm in diameter, and tumor growth was measured in two dimensions using calipers, and tumor volume was calculated using the formula tumor volume (in mm^3) = length × $width^2$ × 0.5.

Serum ELISA for VEGF. Blood was collected at the time of tumor harvest from mice with Vec and VEGF+ tumors. The serum was analyzed by ELISA for VEGF levels.

PECAM Immunohistochemistry of Tumor Sections. Cryopreserved tumor tissue sections of Vec and VEGF+ tumors were fixed in cold acetone on ice for 5 min and blocked with PBS containing 5% BSA and rabbit serum. The sections were immunostained using a rat antimurine PECAM antibody (a generous gift from Dr. Steven Albelda; University of Pennsylvania, Philadelphia, PA), an antirat secondary antibody (Vector Laboratories, Burlingame, CA), the ABC Elite kit, and Vector VIP Peroxidase Substrate kit (Vector Laboratories). A tumor tissue section of each type that was not exposed to primary antibody was used as negative control for PECAM immunostaining. The slides were viewed and photographed under a light microscope at a total magnification of ×200.

MVD Measurements. MVD was assessed by light microscopy in Vec and VEGF+ tumor tissue sections. Areas of most intense vascularization were selected by scanning PECAM-immunostained tumor sections under a light microscope using a ×100 objective. Individual microvessels were then counted within a ×200 field equal to 0.95 mm^2 in area. Branches arising from vessels were counted as individual vessels. Any brown-staining endothelial cell or endothelial cell cluster that was clearly separate from adjacent microvessels and tumor cells was considered a single countable microvessel. Vessel lumens, although sometimes present, were not necessary for a structure to be defined as a microvessel. All counts were performed separately by two investigators. The mean of five fields was computed for each tumor section, and SDs were computed.

Tumor pO_2 Measurements by Eppendorf Electrode. Sixteen athymic nude mice, aged 6–8 weeks, received injection in the right flank with 5×10^6 Vec or VEGF+ cells. When the tumors reached 10–12 mm in greatest dimension, mice were anesthetized with ketamine-xylazine, and tumor pO_2 was measured using a fine-needle probe that was developed by the Eppendorf Corp. (Eppendorf pO_2 Histograph 6650), which measured oxygen partial pressures in solid tissues. The technique of oxygen histography using this device has been described previously in detail (16). The procedure was as follows: an Ag/AgCl reference electrode was placed on the subject's skin. A small stab wound incision (approximately 2 mm) was made with a #11 blade knife over the tumor because the electrode was not able to penetrate through skin or animal pelt. A calibrated polarographic needle electrode (0.3 mm in diameter) that contained a 12-μm insulated gold electrode was inserted into the tumor at a superficial location. The electrode was oriented such that as it advanced, it transgressed a large portion of the tumor diameter. The probe was driven forward by a computer-controlled micromotor for approximately 1.0 mm and then it retracted by approximately 0.3 mm before making a measurement of oxygen pressure. The net forward motion for each measurement was 0.7 mm, and an oxygen tension reading was taken at each of those steps. Each reading took approximately 1 s to complete. The current between the insulated gold cathode and the reference electrode was proportional to the tissue oxygen tension at the cathode tip. The spatial resolution of the reading was approximately 100 μm. The relative frequencies of the individual pO_2 values were then displayed in a histogram to give the oxygen profile for that needle track in the tissue studied. It has been estimated that somewhere between 20 and 50 measurements/tumor were required to accurately assess the oxygen levels of

the tissue. Because each measurement is taken at 0.7-mm stepwise intervals, a 1-cm probe tract was approximately 12 individual measurements. Therefore, for 1-cm tumors, between two and three passes were made into each tumor in different orientations. The Eppendorf histograph system is programmed to advance continuously in small steps, withdrawing partially to relieve tissue compression before each reading, and is programmed to calculate tissue pO_2 values based on an external calibration and also to summarize the measurements into a frequency histogram with 2.5 Torr bins. Data for the same tumor types were combined for descriptive statistics (SigmaStat; SPSS Inc., Chicago, IL) and also separated into frequency histograms with 2.5 Torr bins.

Tumor pO_2 Measurements by Recessed Probe Microelectrode. Ten athymic nude mice, aged 6–8 weeks, received injection in the right flank with 5×10^6 Vec or VEGF+ cells. When the tumors reached 10–12 mm in greatest dimension, mice were anesthetized with ketamine-xylazine, and tumor pO_2 was measured using recessed microelectrodes (17) that were constructed from metal-filled glass micropipettes plated with gold as described by Buerk (18). Tip diameters were typically <5 μm, with <50 μm deep recesses. The gold cathode was dip coated to apply a Nafion membrane (3% weight in aliphatic alcohols; Aldrich Chemical Co., Chicago, IL). pO_2 microelectrodes were tested for stability and precalibrated at 37°C in room air-equilibrated (149 Torr) and 100% N_2 deoxygenated (0 Torr) in PBS solutions before each experiment. Polarographic currents were measured with a sensitive picoammeter (Model 610C; Keithley Instruments, Cleveland, OH) with microelectrodes polarized at -0.7 V relative to a Ag/AgCl reference. The picoammeter output was low pass filtered and digitized by a computer with 12-bit resolution. Sensitivities ranged between 0.3 and 0.5 picoampere/Torr with 90% time responses typically $<$ 100 ms for a step change in pO_2. The skin surrounding the tumor of mice was sutured onto a stainless steel support ring to eliminate tumor movements with respiration. Small cuts were made in the skin to insert microelectrodes into the tumor at different locations. A heated (37°C) PBS bath equilibrated with 20.9% O_2 was superfused over the measurement site. A grounded Ag/AgCl reference wire was placed under the skin in direct contact with the tumor. Recessed microelectrodes were positioned into the bath above the tumor while viewing through a microscope. The steady-state current in the bath before each penetration was used as the calibration current for converting to appropriate partial pressure units, after correcting for the small residual current at zero pO_2. After each steady-state calibration, the microelectrode was manually inserted approximately 500 μm deep to avoid measurements from shallow tissue locations that would be oxygenated by the bath. The microelectrode was then slowly advanced in 0.5-μm steps using a motor driven micropositioner to a final depth approximately 3 mm from the surface of the tumor, or deeper in some cases. Each penetration required several minutes to reach the maximum depth. The microelectrode was then rapidly pulled back into the bath for another steady-state calibration and repositioned to make another measurement at a different location. Recessed pO_2 microelectrode signals were digitized by a computer at 1 Hz sampling rates and stored for offline data analysis. A data point was obtained for approximately every 5-μm change in position. Over 10 penetrations with tissue pO_2 values at 4000–5000 locations were obtained from each tumor. Data for the same tumor types were lumped together for descriptive statistics (SigmaStat; SPSS Inc.) and also separated into frequency histograms with 2.5 Torr bins.

BF and BV by Sonography and DUS. B-mode and Doppler imaging (including color flow and power) was performed on nine tumor-bearing anesthetized athymic nude mice (four Vec and five VEGF+) using a Siemans Elegra Ultrasound Imaging System [Siemens, Issaquah, WA (19, 20)]. The largest cross-sections of the tumor that were evaluated were identified in saggital and transverse planes. The diameter D_1 and the diameters D_2 and D_3 were measured in the transverse and saggital planes, respectively. These measures were in turn used to compute the volume V of the tumor by the formula: $V = 0.5 * D_1 * D_2 * D_3$. The power Doppler images were recorded on a videotape at the lowest possible wall filter without causing aliasing of the images. The Doppler gain was kept constant for all of the studies. After the recording of a power Doppler image, a color Doppler image was recorded in the same plane. Approximately 20–40 planes in both the longitudinal and transverse planes were collected per tumor and analyzed by ultrasound software developed specifically for this purpose. The tumor in each image was identified and outlined by the user in each case. Computer analysis consisted of reading the color palette and assigning a value of 0 to the "lowest" and 100 to the "highest" color in the palette bar. With this information, the computer constructed a "look up" table from the hue, saturation, and brightness values of the colors present in the palette bar. Using the look-up table, the computer identified the colored pixels within the region outlined by the user. It counted the number of colored pixels (n) and the number of pixels identified as the tumor (N). It also measured the color level of each pixel determined by the hue, saturation, and brightness values. Using these measurements, the flow indices, VD, MCL, and CWFA, were calculated for each color and power Doppler image.

If i represents a color pixel, and C_i represents its color level, then the VD (also referred to as the fractional area of perfusion) and MCL were determined by the formulas

$$\mathrm{VD} = \frac{100 * \sum_{i=1}^{n} i}{N}$$

= percentage area of the tumor occupied by blood vessels, and

$$\mathrm{MCL} = \frac{\sum_{i=1}^{n} C_i}{nG},$$

where G represents the scaling factor, with values ranging from 0 to 1, for the color gain used during imaging. As described above, this level was kept fixed for all studies. The product of the two parameters was used to calculate CWFA as shown below.

$$\mathrm{CWFA} = \mathrm{MCL} \times \mathrm{VD}$$

The physical meaning of the measurement VD is straightforward because it represents the relative area of perfusion. The meaning of the term MCL, varied depending on whether it was derived from color or power Doppler images. The MCL measurements from color Doppler images are a measure of mean velocity of local BF. The MCL measurements derived from power Doppler images represented the number of RBCs moving above a threshold velocity. If one assumes local hematocrit in these small blood vessels to be equal to systemic hematocrit, power Doppler MCL can be regarded as related to BV (or, more appropriately, related to the log of BV because the signals are often log-compressed) moving above a threshold velocity.

The relationship between MCL and physiological parameters (mean flow velocity and BV) should be viewed as semiquantitative because of several variables: the angle between a blood vessel and the direction of ultrasound; the choice of scale maximum; filters and color write priority threshold; and the interpolation, averaging, and other image processing algorithms used internally within a scanner to display images for optimal viewing. However, if the imaging parameters are kept constant throughout the study, as was the case in this study, the influence of these variables can be significantly reduced. Under these circumstances, the data provide a meaningful comparison of the flow characteristics through two different tissue types or before and after treatment with various agents. CWFA combines the MCL and VD information. In the case of color Doppler, CWFA (flow mean velocity $\times$ area of perfusion) corresponds to the BF through the tumor. Similarly, the CWFA for power Doppler images (product of MCL and VD) is a measure of the "moving" BV within the tissue.

BF and Blood OS by DLS. Thirteen athymic tumor-bearing nude mice (seven VEGF+ and six Vec) were anesthetized with an i.p. injection of ketamine-xylazine, and then relative BF and blood OS in the two tumor types were measured using a combination of two NIR diffuse optical techniques (21, 22). Briefly, diffuse correlation spectroscopy (or flowmetry) was used to determine relative BF; this method essentially measures the optical phase-shifts caused by moving blood cells. NIR absorption spectroscopy was used concurrently to measure tissue absorption at two different wavelengths. These measurements of diffuse light reflection enabled us to determine the hemoglobin concentration and blood OS of the same tumor tissue we probed simultaneously by the flow method. The instrument used noncontacting sources of NIR light derived from laser diodes; source photons were delivered centrally into the tumors. Four detection fibers were arranged on a square

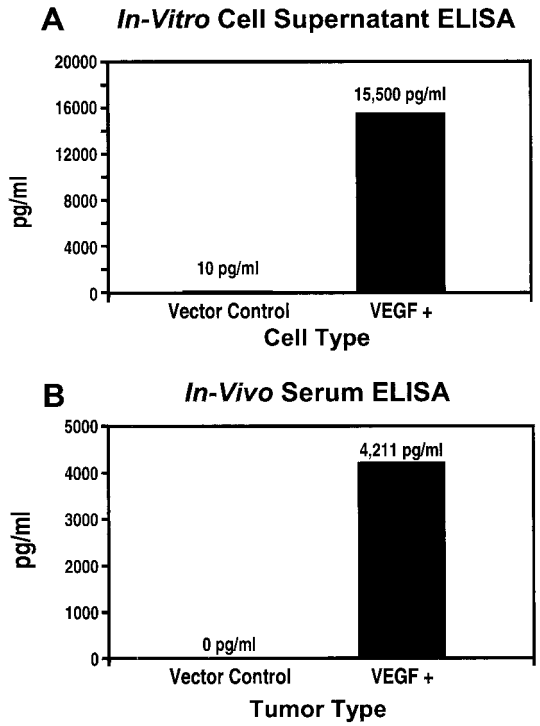

Fig. 1. VEGF levels in cell supernatants (*A*) and serum (*B*) by ELISA in Vec and VEGF+ cell lines and tumors. VEGF+ cells showed a 100-fold higher VEGF compared with Vec cells. VEGF levels were detectable (4211 pg/ml) in the serum of mice carrying VEGF+ tumors and undetectable in the serum of mice carrying Vec tumors.

around the central source fiber. The source-detector separation distance was fixed at 3.3 mm. The diffuse light transmitted through the tumors was captured by this radial distribution of light detectors. BF was computed from the temporal decay of the diffuse light intensity temporal autocorrelation function. Typically this autocorrelation function decays exponentially. Its decay rate, Γ (s^{-1}), depends on a parameter α, proportional to the tissue BV fraction, and on the motion of blood cells. Depending on the physical model used, the decay rate is proportional to one of the following parameters, which are related to the average motion of the RBCs: a Brownian diffusion coefficient, D_B (cm^2/s); or a mean-square flow velocity, V^2 [$(cm/s)^2$] (21, 22). We have generally found that our autocorrelation function fits are better when using the model containing the Brownian diffusion coefficient, D_B. Relative changes in D_B correspond to relative changes in BF. The blood OS was computed from the diffusely reflected light signals at 830 nm (oxyHb peak) and at 750 nm (deoxyHb peak). This calculation assumes that the dominant absorbers at these wavelengths are oxyhemoglobin and deoxyhemoglobin, and that the smaller, water and lipid contributions to the signal remain constant.

Statistical Analysis. The Graphpad Instat and Microsoft Excel software were used to perform statistical analysis on the DUS and DLS and MVD data. Statistical analyses for the Eppendorf and recessed oxygen microelectrode have been described in their respective sections.

RESULTS

NIH1286/VEGF+ cell supernatants expressed a >1000-fold higher VEGF (15,500 pg/ml) when compared with the vector-only cell line (10 pg/ml; Fig. 1*A*). Oxygen consumption rates were found to be equivalent in the VEGF+ and Vec cell lines (0.36 0.06 nmol oxygen/min/10^5 for VEGF+ cells and 0.40 0.09 nmol oxygen/min/10^5 cells for Vec cells). Five million cells of either line were then injected s.c. into athymic nude mice, and tumors were allowed to grow until they reached 10–14 mm in maximum dimension. Whereas VEGF+ tumors appeared pink in color, tumors produced by injecting Vec cells were grayish blue in color (Fig. 2). A plausible explanation for these observations is increased vascularity in the VEGF-transfected tumors. The VEGF+ tumor type had higher growth rates when compared with the Vec tumor type. Whereas the VEGF+ tumors ($n = 28$) reached 70–80 mm^2 between day 9 and day 15 after tumor inoculation, the control tumor type ($n = 27$) reached 60–70 mm^2 between day 13 and day 20 after tumor inoculation. Serum was collected and analyzed by ELISA for VEGF levels when the tumors were 10–14 mm in maximum dimension. Whereas these levels were undetectable in the serum of Vec tumor-bearing mice, the serum from mice carrying VEGF+ tumors showed a VEGF level of 4211 pg/ml (Fig. 1*B*). Both tumor types were then harvested from anesthetized mice, frozen in OCT, cryosectioned, and analyzed for MVD by PECAM immunohistochemistry. The MVD was determined to be 72 15 for VEGF+ tumors and 39 4 for the Vec tumor type (Fig.

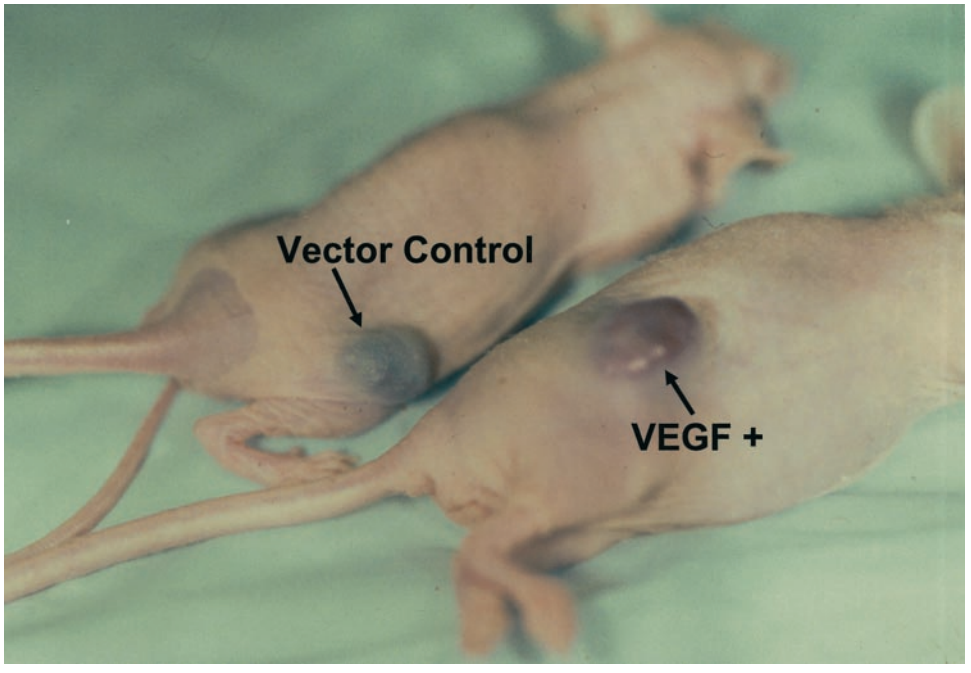

Fig. 2. Photograph of mice with VEGF+ or Vec tumors. VEGF+ tumors were *pale pink* in color due to the hypervascular nature of these tumors, and in contrast, the Vec tumors were *grayish blue* in color.

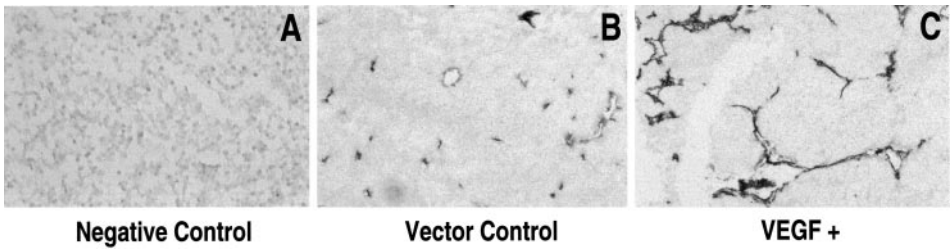

Fig. 3. Photomicrographs of tumor tissue sections immunostained for PECAM. Negative control without primary antibody, *A*; Vec tumor tissue section, *B*; VEGF+ tumor tissue section, *C*. The VEGF+ tumor tissue section showed the hypervascular nature of these tumors.

3). This consistent and reproducible difference in VD between the two tumor types was used as a model system to delineate the tumor oxygen status including tumor tissue pO_2, relative BF, BV, and blood OS using the recessed oxygen microelectrode, DUS, and DLS.

Direct tumor tissue pO_2 measurements were obtained using recessed pO_2 microelectrodes in 10 tumors (5 VEGF+ and 5 Vec tumors) and the Eppendorf system in 16 tumors (7 Vec and 9 VEGF+ tumors) to make a comparison between the data obtained from the two methods. Frequency and cumulative distributions from these experiments are shown in Fig. 4. Eppendorf tissue pO_2 distributions for both tumor types were shifted to the left, with a larger fraction of values in the lowest bin (0–2.5 Torr) compared with recessed pO_2 microelec-

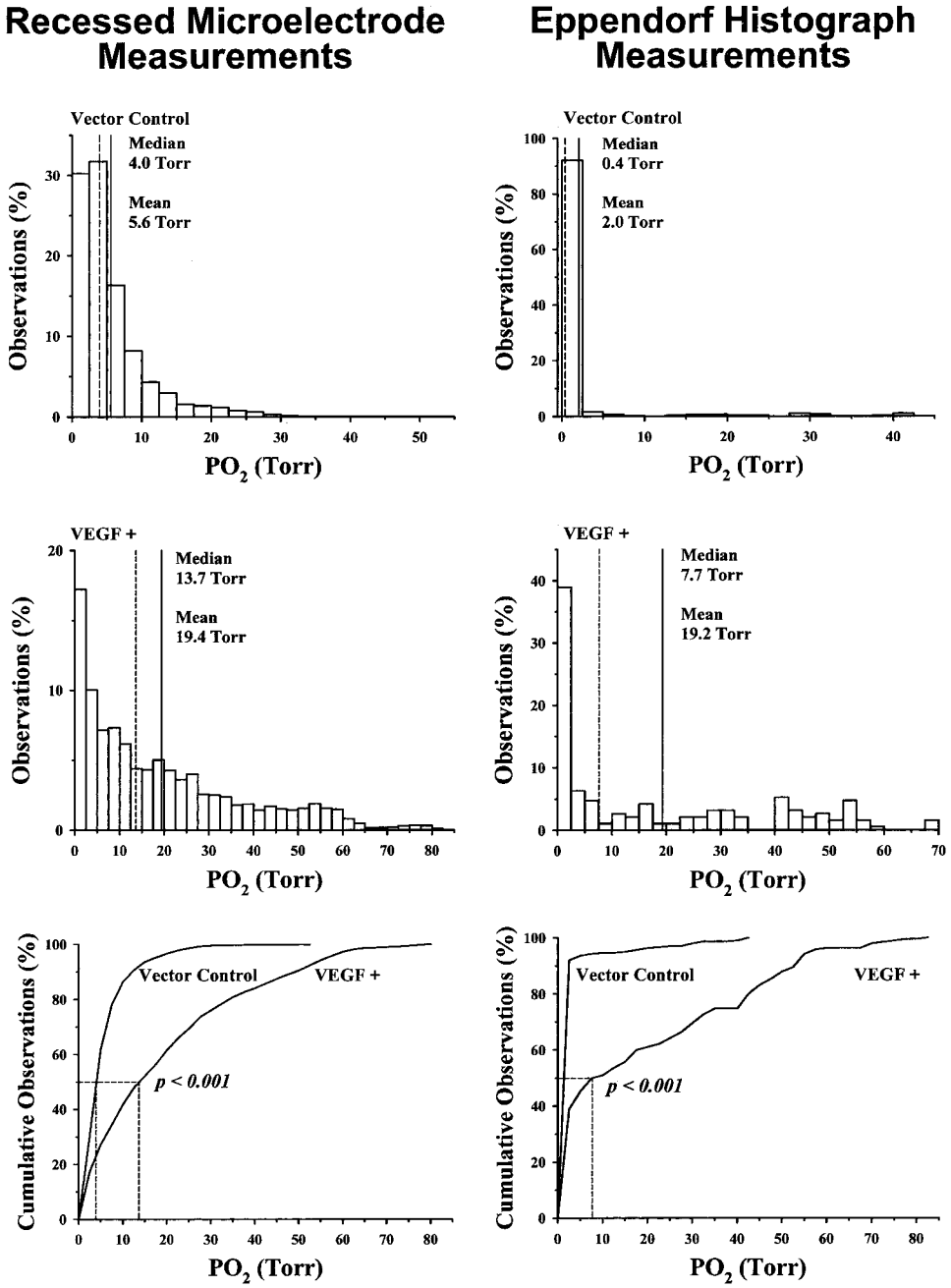

Fig. 4. Frequency histograms for tissue PO_2 distributions measured by recessed PO_2 microelectrodes (*left panels*) and Eppendorf histograph (*right panels*) for Vec tumors (*top panels*) and VEGF+ tumors (*middle panels*), with comparison of cumulative frequency distributions for the two tumor types (*bottom panels*). Median tumor tissue pO_2 values measured with recessed pO_2 microelectrodes were found to be significantly higher for VEGF+ tumors (*dashed lines, bottom left panel*), but no statistical comparison could be made with the Eppendorf method.

Table 1 *Statistics for pO_2 microelectrode measurements*

Tumors (*n*)	Electrode	Median	Mean	SD	SE	Values	Range	Skewness	Kurtosis
Vector control (5)	Recessed	4.0	5.6	5.5	0.030	25,417	0–52	2.6	10
VEGF+ (5)	Recessed	14[a]	19	18	0.12	22,983	0–81	1.1	0.35
Vector control (9)	Eppendorf	0.40	2.0	6.4	0.38	299	0–42	4.5	21
VEGF+ (7)	Eppendorf	7.1[a]	19	22	1.6	190	0–85	0.87	−0.43

[a] $P < 0.001$, Mann-Whitney rank-sum test.

trode distributions. Slightly >90% of the values were below 2.5 Torr for the vector-only containing tumors ($n = 9$), with no values above 42 Torr measured by the Eppendorf histograph. Median and mean tissue pO_2 values were 0.40 and 2.0 Torr, respectively. No values above 52 Torr were measured with recessed pO_2 microelectrodes in the vector-only tumors ($n = 5$), but the median tissue pO_2 was higher at 4.0 Torr. Approximately 14% of recessed pO_2 microelectrode values were >10 Torr compared with 6.4% >10 Torr as determined by the Eppendorf. pO_2 measurements with both types of electrodes clearly showed that VEGF+ tumors were better oxygenated than Vec tumors. However, median pO_2 measurements made with recessed pO_2 microelectrodes were higher than those obtained with the Eppendorf histograph. The median pO_2 was <7.7 Torr with the Eppendorf but was 14 Torr using recessed pO_2 microelectrodes. Whereas the distributions are different at low pO_2, both are similar at higher ranges, with 25% of Eppendorf values and 19% of recessed pO_2 microelectrode values above 35 Torr. The mean values were nearly the same.

Descriptive statistics for the recessed pO_2 microelectrode measurements are summarized in Table 1. pO_2 distributions measured with recessed microelectrodes for the two tumor groups were analyzed by a Kolmogorov-Smirnov normality test. The data sets were not described by normal distributions, as indicated by the skewness and kurtosis values. Therefore, a Mann-Whitney rank-sum test was used to compare medians for the two groups. VEGF-transfected tumors had a significantly higher ($P < 0.001$) median tissue pO_2 than vector-only containing tumors (Table 1).

In a second set of experiments, nine tumor-bearing athymic nude mice (five VEGF+ and four Vec) were used to measure color level from the color and power Doppler images (Figs. 5 and 6). These color levels correspond to tumor BV and BF, respectively. Fig. 5 compares the color and power Doppler images of VEGF+ and Vec tumors. The *left column* represents the gray-scale images, the *middle column* shows the color Doppler images (BF), and the *right column* shows power Doppler images (BV). There is a marked difference in the number of blood vessels and intensity of color/unit area of tumor in VEGF+ tumors when compared with the Vec tumors. Fig. 6 is a quantitative representation of these results, which shows that VEGF+ tumors have a relative mean BF that is 3.4 times higher than that of Vec tumors. Whereas the relative BF values varied between 2.4 and 5.2 for VEGF+, they varied between 1.0 and 1.1 for Vec. The median values were 3.3 and 1.1 for VEGF+ and Vec, respectively ($P_2 = 0.0079$). Relative mean BV was 6.8 2.3 in VEGF+ tumors and 1.2 0.45 in Vec tumors (Fig. 6; $P_2 = 0.0059$). Whereas the relative BV values varied between 4.2 and 8.9 for VEGF+, they varied between 0.93 and 1.9 for Vec tumors. The median values were 7.7 and 1.1 for VEGF+ and Vec tumor types, respectively.

In a third set of experiments, 13 tumor-bearing athymic nude mice (7 VEGF+ and 6 Vec) were used to measure relative mean tumor BF and relative mean blood OS variation using DLSs. Relative mean BF, as parameterized by D_B (in units of 1×10^{-8} cm^2/s) was determined to be 5.6 1.8 in VEGF+ and 1.7 0.60 in Vec tumors (Fig. 7; $P_2 = 0.0012$). The minimum and maximum measured values of D_B were 3.4 and 8.6 for VEGF+ tumors and 0.9 and 2.4 for Vec tumors, respectively. The corresponding median BFs were 5.4 and 1.8. Mean blood OS was found to be 0.7 0.1 and 0.4 0.1 in the two tumor types, respectively (Fig. 7; $P_2 = 0.0016$). The minimum and maximum blood OS values were 0.53 and 0.91 for VEGF+ and 0.21 and 0.56 for Vec, respectively. The median blood OSs were 0.71 and 0.44, respectively. Table 2 summarizes all of the data obtained from DUS and DLS. Taken together, the data showed that the VEGF-transfected

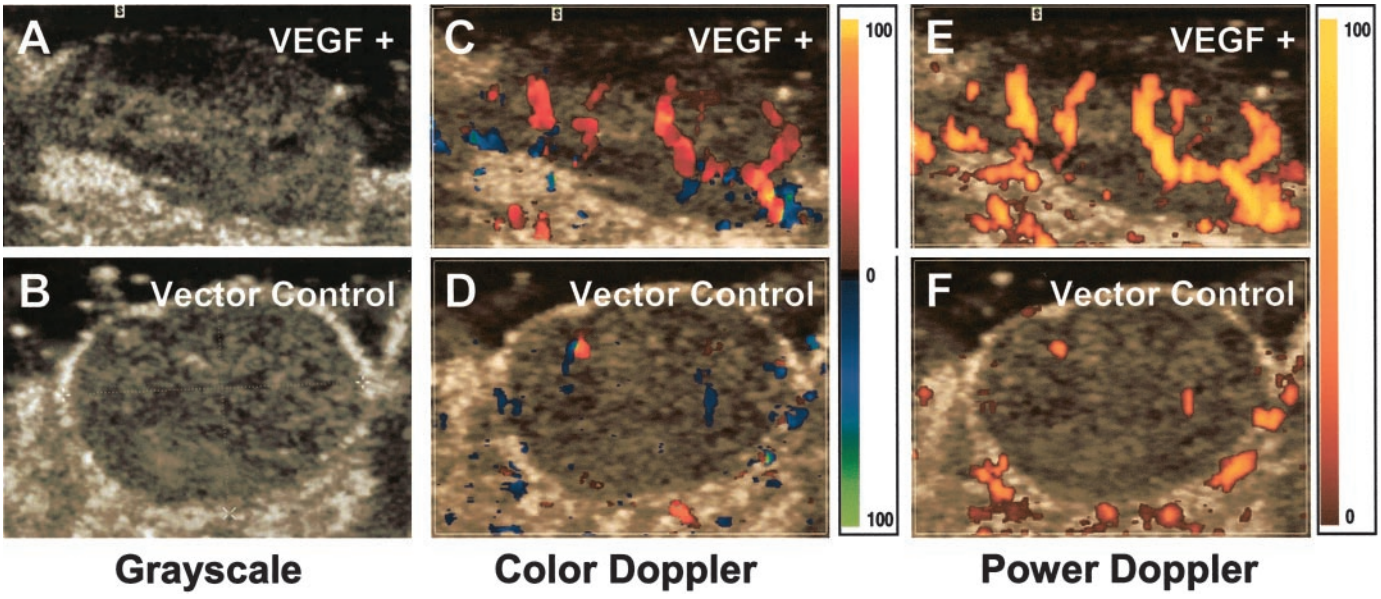

Fig. 5. Color and power Doppler images of VEGF+ (*top panels*) and Vec (*bottom panels*) tumors. The *left column* represents the gray-scale images. The *middle column* shows the color Doppler images (BF), and the *right column* shows power Doppler images (BV). There is a marked difference in the number of blood vessels and intensity of color/unit area of tumor in VEGF+ tumors when compared with the Vec tumors.

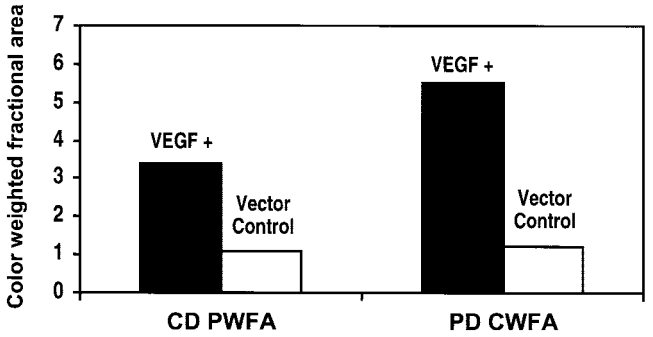

Fig. 6. A quantitative representation of color and power Doppler data from VEGF+ and Vec tumors. Color level was computer analyzed by comparison with the color palette on the image. For PD images, the color in the palette was equally divided between its lowest and highest levels on a scale of 0–100. For the CD images, the colors red and blue (which represent BF in two different directions) were each assigned a scale of 0–100. VEGF+ tumors showed a relative mean BF that was 3.4 times higher than that of Vec tumors and a mean BV that was 5.5 times higher than that of Vec tumors. PD = power Doppler. CD = color Doppler.

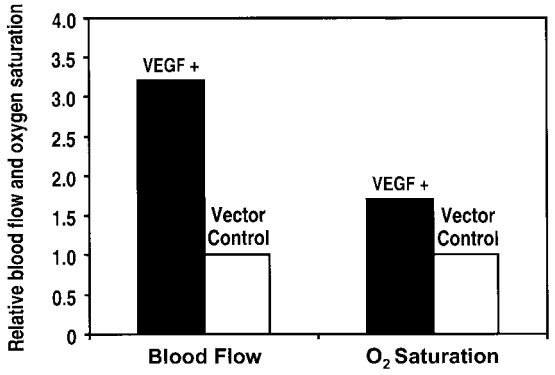

Fig. 7. Relative mean tumor BF and relative mean blood OS variation in VEGF+ and Vec tumors using DLSs. Relative mean BF, as parameterized by D_B (in units of 1×10^{-8} cm^2/s) was determined to be 3.3-fold higher, and the mean blood OS was found to be 1.75-fold higher in VEGF+ tumors than in Vec tumors.

tumor type, as expected, had an overall higher tumor oxygen status compared with the vector-only counterpart.

DISCUSSION

There are many reasons with clinical relevance to obtain an assessment of a solid tumor's oxygen status represented by MVD, BF, BV, OS, and tumor tissue pO_2. Hypoxic tumors are known to be more resistant to treatment with chemotherapeutics, radiation therapy, and photodynamic therapy (3). There is evidence, in a variety of neoplasms, that hypoxic tumors are more aggressive and have a worse prognosis independent of treatment response (2). Furthermore, treatment with antiangiogenic agents may lead to a change in tumor vascularity and oxygenation without a change in tumor size (5). Reliable measurement of change in vascularity is, therefore, important to screen for the effectiveness of antiangiogenic agents. Delineation of pretherapeutic tumor oxygen status may also help in developing patient-specific treatment strategies.

There are many obstacles to obtaining a reliable measurement of tumor oxygen status and tumor vascularity. First, there is a great deal of heterogeneity within solid tumor nodules. Second, a variety of noninvasive imaging techniques that have been developed and used to measure oxygenation status are hard to validate with direct measurements (6–13). The best reported direct measurement of tumor oxygenation uses the commercially available Eppendorf microelectrode, which has its limitations (16). The present study provides an integrated approach to defining the oxygen status of the tumor and is validated by direct measurements. We used a reproducible s.c. human tumor xenograft model for the purpose. Tumors were grown from a human melanoma cell line that was transfected with either hVEGF or its vector alone to provide two tumor types, one that was more vascular than the other, in which to measure and compare tumor vascularity and oxygenation. We validated the results with direct oxygen measurements made with a recessed oxygen microelectrode and also compared them with direct measurements made with the Eppendorf electrode.

The Eppendorf pO_2 electrode has been considered the "gold standard" for measuring tumor oxygen tension (23), although this has been questioned (24). Because the technology has been around for several decades, it has been the only technique that could directly measure tumor tissue pO_2. However, despite the relative ease with which the device can be used, there are a number of important problems that need to be addressed. Buerk (25) discusses some of these issues and the advantages for using smaller recessed pO_2 microelectrodes to make tissue pO_2 measurements. The potential for tissue damage by the Eppendorf needle is a problem, particularly for tumors that are relatively small. Miniaturized electrochemical sensors have two major advantages compared with larger electrodes: (*a*) faster time responses; and (*b*) finer spatial resolution. Miniaturization can also minimize tissue damage and microcirculatory disturbances by the microsensor, decreasing possible distortion of the physiological measurement (25). With the much larger dimensions of the Eppendorf pO_2 electrode, we believe that the most likely explanation for the differences in tumor tissue pO_2 distributions is the greater probability for damage to capillaries and small blood vessels compared with damage that might be caused by the smaller tip of the recessed pO_2 microelectrodes. Although multiple sampling sites with the recessed microelectrode may allow the best direct assessment of tumor oxygenation without disruption of the microvasculature, pO_2 measurement using the glass microelectrode cannot be used clinically in its present form and will need to be further developed before it can be used in patients. This suggests that there is still a persisting requirement for valid and

Table 2 *DUS and DLS data analysis*

	NIH1286	*n*	Mean	SD	SE	Median	Low 95% CI[a]	Up 95% CI	VEGF+ Control	*P* (1-tail)	*P* (2-tail)
Power Doppler (BV)	VEGF+	5	6.8	2.3	1.0	7.7	4.0	9.6	5.5	0.0030[b]	0.0059[b]
	Vector control	4	1.2	0.45	0.2	1.1	0.52	1.9			
Color Doppler (BF)	VEGF+	5	3.4	1.1	0.48	3.3	2.1	4.8	3.3	0.0040[b]	0.0079[b]
	Vector control	4	1.1	0.0096	0.0048	1.1	1.0	1.1			
DLS (BF)	VEGF+	7	5.6E-08	1.8E-08	6.9E-09	5.4E-08	3.9E-08	7.3E-08	3.2	0.00060[b]	0.0012[b]
	Vector control	6	1.7E-08	6.5E-09	2.6E-09	1.8E-08	1.1E-08	2.4E-08			
DLS (OS)	VEGF+	7	0.71	0.13	0.047	0.71	0.60	0.82	1.7	0.00080[c]	0.0016[c]
	Vector control	6	0.42	0.12	0.048	0.44	0.30	0.55			

[a] CI, confidence interval.
[b] Unpaired *t* test with Welch correction.
[c] Unpaired *t* test.

reliable oxygen-sensing probes that combine the advantages of the two types of electrodes used in this study. This invasive technique using either type of probe, however, does not provide much direct information on BF, BV, or OS. We assessed these parameters of tumor vascularity using DUS and DLS. Ultrasound measurements made with power Doppler imaging provide an estimate of total BV in tumors. Our measurements show that the color-weighted power Doppler signal from VEGF-transfected tumors was 5.5 times stronger than that from the Vec tumors. These results suggest that the VEGF tumors are approximately 5.5 times more vascular than the control tumor type. However, MVD measurements show that the VEGF-transfected tumors have only a 2-fold higher VD when compared with the controls. One plausible explanation for this discrepancy is that the VEGF-transfected tumor types have blood vessels that have a larger diameter and therefore hold greater BV/mm^3 tumor than the vector-only containing control tumor type. In our model system, blood vessels in the VEGF-transfected clone were not only more numerous but also appeared larger than those in the control tumors (Fig. 3). The diffuse optical measurements gave clear signals that differentiated the two tumor types in terms of BF. The optical flow measurements are readily compared with the ultrasound flow measurements, and the optical blood OS may be analyzed in the context of the electrode measurements of tissue oxygen. It is most appropriate to compare the differential changes or ratios because the quantities measured by the different techniques are not precisely the same. Diffuse optical correlation measurements gave a mean BF ratio (VEGF+/Vec−) of 3.2; thus the VEGF tumors clearly exhibited a substantially increased blood perfusion. This result can be compared with BF measured by DUS, which represents a product of mean color Doppler measurements and fractional area Doppler measurements. The corresponding ultrasound flow ratio is 3.3, which is essentially identical to the flow rate measured by DLS. This high degree of correlation is surprising because the diffuse optical probes are sensitive to all tissue flow including capillary contributions, whereas the ultrasound measurement threshold is about 1 cm/s and thus does not directly probe the capillaries. The consistent values suggest that the flow changes in the larger vessels are strongly coupled to changes in capillary flow. The ultrasound BV/BF ratios for the VEGF and control tumor types are 2.0 and 1.2, respectively, indicating that the VEGF-transfected tumor type has "sluggish flow" relative to the vector control. This observation is substantiated by earlier BF and BV studies on other VEGF-transfected tumors cited in the literature (26) and further validates the use of DUS for determining tumor BF and BV.

In the context of blood OS measurements, the optical measurements probe blood, whereas the electrode measurements directly probe oxygen as a gas dissolved in tumor tissue. The mean blood oxygen ratio is 1.7 by DLS; again we see that the VEGF tumors are substantially more oxygenated than their counterparts. The electrode measurements give this same qualitative trend, although the actual ratio is larger (3.6) as an assessment of tissue oxygen. If the number of vessels is identical in the two tumor types, then there should be a good correlation between the oxygenation in the tissue and the oxygenation in the blood vessels supplying the tissue. However, when the OS within the blood is higher and the number of vessels in the VEGF tumor is almost double that of the control tumor type, then it should be expected that the disparity between blood oxygenation and tissue oxygenation will be amplified in the hypervascular tumor type as appropriately indicated by our results.

It is a well-established fact that tumor oxygen status is also dependent on cellular oxygen consumption rate. In our study, the VEGF+ and Vec cell lines were found to have equivalent oxygen consumption rates/tumor cell. Therefore, with the VEGF+ tumor type having higher BF, BV, blood OS, and microvascular density than the control phenotype and equivalent oxygen consumption rates, it is conceivable that the VEGF+ tumor type would have a higher tumor growth rate when compared with the Vec counterpart due to greater availability of oxygen. The VEGF+ tumor growth rate was found to be significantly higher than that of the Vec tumor type, as predicted from the integrated approach tumor oxygen status data.

Although the integrated approach to delineating tumor oxygen status can be a powerful tool in tumor therapy, it has its limitations. Whereas it has the potential to provide useful information in early-stage disease in many types of cancers, such as the identification of the unique pathophysiological parameter that is most relevant for the behavior of malignancies, it may become impossible to carry out when there is extensive metastatic spread. It also appears that tumors that are very large or very small may not be ideal for such a study because both DUS and DLS are noninvasive methods, and the depth of penetration they give is limited. Furthermore, data from oxygen profiles of several different tumor types need to be analyzed to determine whether it is possible to combine the individual data to arrive at a unique value that represents the oxygen status of a tumor. Such values could then be compared against thresholds that would have to be reached for optimal response to the different tumor treatment modalities. DUS and DLS in the present study were used to give relative BV and BF. These techniques could be further refined and standardized to yield absolute values of BV and BF in tumors. Nevertheless, given the central role that tumor oxygenation plays in the pathophysiology of tumors and therefore in prognosis and in the prediction of the tumor's response to treatment, it is relevant and imperative to resolve the shortcomings of such an integrated approach, given the heterogeneity and complexity in tumor oxygenation.

ACKNOWLEDGMENTS

We are grateful to Dr. Steve Tuttle (Department of Radiation Oncology, University of Pennsylvania) for assistance with the Clark oxygen electrode measurements.

REFERENCES

1. Brown, J. M., and Giaccia, A. J. The unique physiology of solid tumors: opportunities (and problems) for cancer therapy. Cancer Res., *58:* 1408–1416, 1998.
2. Vaupel, P., Kelleher, D. K., and Hockel, M. Oxygen status of malignant tumors: pathogenesis of hypoxia and significance for tumor therapy. Semin. Oncol., *28:* 29–35, 2001.
3. Dewhirst, M. W., Klitzman, B., Braun, R. D., Brizel, D. M., Haroon, Z. A., and Secomb, T. W. Review of methods used to study oxygen transport at the microcirculatory level. Int. J. Cancer, *90:* 237–255, 2000.
4. Vaupel, P., and Hockel, M. Hypoxia in cervical cancer: pathogenesis, characterization, and biological/clinical consequences. Zentralblatt fur Gynakologie, *123:* 192–197, 2001.
5. Ellis, L. M., Liu, W., Fan, F., Jung, Y. D., Reinmuth, N., Stoeltzing, O., Takeda, A., Akagi, M., Parikh, A. A., and Ahmad, S. Synopsis of angiogenesis inhibitors in oncology. Oncology (Huntingt.), *16:* 14–22, 2002.
6. Wilson, D., and Cerniglia, G. Oxygenation of tumors as evaluated by phosphorescence imaging. Adv. Exp. Med. Biol., *345:* 539–547, 1994.
7. Helmlinger, G., Yuan, F., Dellian, M., and Jain, R. K. Interstitial pH and pO_2 gradients in solid tumors *in vivo*: high-resolution measurements reveal a lack of correlation. Nat. Med., *3:* 177–182, 1997.
8. Dewhirst, M. W., Ong, E. T., Braun, R. D., Smith, B., Klitzman, B., Evans, S. M., and Wilson, D. Quantification of longitudinal tissue pO_2 gradients in window chamber tumours: impact on tumour hypoxia. Br. J. Cancer, *79:* 1717–1722, 1999.
9. Howe, F. A., Robinson, S. P., and Griffiths, J. R., Modification of tumour perfusion and oxygenation monitored by gradient recalled echo MRI and 31P MRS. NMR Biomed., *9:* 208–216, 1996.
10. Mueller-Klieser, W., Vaupel, P., Manz, R., and Schmidseder, R. Intracapillary oxyhemoglobin saturation of malignant tumors in humans. Int. J. Radiat. Oncol., *7:* 1397–1404, 1981.
11. Parliament, M. B., Chapman, J. D., Urtasun, R. C., McEwan, A. J., Golberg, L., Mercer, J. R., Mannan, R. H., and Wiebe, L. I. Non-invasive assessment of human tumour hypoxia with ^{123}I-iodoazomycin arabinoside: preliminary report of a clinical study. Br. J. Cancer, *65:* 90–95, 1992.
12. Rasey, J. S., Koh, W. J., Evans, M. L., Peterson, L. M., Lewellen, T. K., Graham, M. M., and Krohn, K. A. Quantifying regional hypoxia in human tumors with positron

emission tomography of [^{18}F]fluoromisonidazole: a pretherapy study of 37 patients. Int. J. Radiat. Oncol., *36:* 417–428, 1996.
13. Chapman, J. D., Engelhardt, E. L., Stobbe, C. C., Schneider, R. F., and Hanks, G. E. Measuring hypoxia and predicting tumor radioresistance with nuclear medicine assays. Radiother. Oncol., *46:* 229–237, 1998.
14. Chaplin, D., Olive, P., and Durand, R. Intermittent blood flow in a murine tumor: radiobiological effects. Cancer Res., *47:* 597–601, 1987.
15. Evans, S., Jenkins, W., Joiner, B., Lord, E., and Koch, C. 2-Nitroimidazole (EF5) binding predicts radiation resistance in individual 9L s.c. tumors. Cancer Res., *56:* 405–411, 1996.
16. Kallinowski, F., Zander, R., Hoeckel, M., and Vaupel, P. Tumor tissue oxygenation as evaluated by computerized-pO_2-histography. Int. J. Radiat. Oncol., *19:* 953–961, 1990.
17. Whalen, W. J., Riley, J., and Nair, P. A microelectrode for measuring intracellular pO_2. J. Appl. Physiol., *23:* 798–801, 1967.
18. Buerk, D. G. Biosensors: Theory and Applications, pp. 95–123. Lancaster, PA: Technomic Publishing Co., Inc., 1993.
19. Sehgal, C. M., Arger, P. H., Rowling, S. E., Conant, E. F., Reynolds, C., and Patton, J. A. Quantitative vascularity of breast masses by Doppler imaging: regional variations and diagnostic implications. J. Ultras. Med., *19:* 427–440, 2000.
20. Sehgal, C. M., Arger, P. H., Silver, A. C., Patton, J. A., Saunders, H. M., Bhattacharyya, A., and Bell, C. P. Renal blood flow changes induced with endothelin-1 and fenoldopam mesylate by quantitative Doppler US: initial results in a canine study. Radiology, *219:* 419–426, 2001.
21. Cheung, C., Culver, J. P., Takahashi, K., Greenberg, J. H., and Yodh, A. G. *In vivo* cerebrovascular measurement combining diffuse near-infared absorption and correlation spectroscopies. Phys. Med. Biol., *46:* 2053–2065, 2001.
22. Boas, D. A., and Yodh, A. G. Spatially varying dynamical properties of turbid media probed with diffusing temporal light correlation. J. Opt. Soc. Am. A., *14:* 192–215, 1997.
23. Stone, H. B., Brown, J. M., Phillips, T. L., and Sutherland, R. M. Oxygen in human tumors: correlations between methods of measurement and response to therapy. Radiat. Res., *136:* 422–434, 1993.
24. Olive, P. L., Bananth, J. P., and Aquino-Parsons, C. Measuring hypoxia in solid tumours: is there a gold standard? Acta Oncol., *40:* 917–923, 2001.
25. Buerk, D. G. Measuring tissue pO_2 with microelectrodes. *In:* C. K. Sen and G. L. Semenza (eds.), Oxygen Sensing, Methods in Enzymology. San Diego, CA: Elsevier Science, in press.
26. Oku, T., Tjuvajev, J. G., Miyagawa, T., Sasajima, T., Joshi, A., Joshi, R., Finn, R., Claffey, K. P., and Blasberg, R. G. Tumor growth modulation by sense and antisense vascular endothelial growth factor gene expression: effects on angiogenesis, vascular permeability, blood volume, blood flow, fluorodeoxyglucose uptake, and proliferation of human melanoma intracerebral xenografts. Cancer Res., *58:* 4185–4192, 1998.